DOI: 10.1002/chem.200601256

# $Mo_{15}S_{20}$: First Evidence of a New Molybdenum Cluster Type in a Metastable Solid-State Compound

**Dialla Salloum,[a] Régis Gautier,[b] Michel Potel,[a] and Patrick Gougeon*[a]**

**Abstract:** The $Mo_{15}S_{20}$ compound was obtained by thermal decomposition of the metastable binary $Mo_{15}S_{19}$ in sealed silica tube at temperatures above 500 °C. Its crystal structure was solved and refined from a two-component composite crystal by X-ray diffraction in the hexagonal space group $P6_3/m$ and consists of an equal mixture of the original $Mo_9S_{27}$ cluster unit and the classical one $Mo_6S_8S_6$ interconnected through Mo–S bonds. The Mo core of the $Mo_9S_{27}$ unit is totally new and formed a tricapped trigonal prism. Quantum chemical calculations carried out in order to understand these trends as well as magnetic susceptibility measurements are also reported. The title compound becomes superconducting below 5 K.

**Keywords:** ab initio calculations · cluster compounds · electronic structure · molybdenum · solid-state structures · superconductors

## Introduction

Chalcogenides containing low-valent molybdenum are generally characterized by metal clusters of diverse sizes and geometries[1] and have been studied intensively in the last three decades because of their exceptional physical properties.[2] In such compounds, the Mo clusters can accept a variable number of electrons (often called metallic electrons (ME)) available for Mo–Mo bonding. The ME count, which governs the physical properties, can be modified through topotactic reduction–oxidation reactions at low temperatures. This is particularly well exemplified by the silver deinsertion from $Ag_{3.6}Mo_9Se_{11}$ that yields the isomorphous metastable compound *o*-$Mo_9Se_{11}$.[3] The latter phase is a superconductor with 32 ME per $Mo_9$ cluster, while the parent ternary compound is a semiconductor and has 35.6 ME per $Mo_9$. Previous work has shown that the indium/molybdenum chalcogenide clusters, such as $InMo_6S_8$, $In_{3.7}Mo_{15}S_{19}$, $In_{3.3}Mo_{15}Se_{19}$, $In_2Mo_{15}Se_{19}$ or $In_2Mo_6Se_6$ are also good candidates for topotactic reduction–oxidation reactions at low temperatures.[4] Indeed, the indium can be removed easily from these ternary compounds by oxidation with $I_2$ or HCl gas to give the corresponding metastable binary compounds. These binary compounds always decompose directly into Mo and $MoS_2$ or $MoSe_2$ generally above 600 °C. We present here the first example of a metastable cluster compound, that is, $Mo_{15}S_{19}$ containing octahedral $Mo_6$ and bioctahedral $Mo_9$ clusters,[5] that decomposes into a new metastable cluster compound $Mo_{15}S_{20}$. This process is accompanied by a modification of the bi-octahedral $Mo_9$ cluster, which adopts a novel form. All measurements were performed on single crystals. An X-ray diffraction study, magnetic susceptibility measurements, and electronic structure calculations of this new compound are reported herein.

[a] Dr. D. Salloum, Dr. M. Potel, Dr. P. Gougeon
UMR CNRS 6226—Sciences Chimiques de Rennes
Université de Rennes 1, Avenue du Général
35042 Rennes (France)
Fax: (+33) 299-635-704
E-mail: patrick.gougeon@univ-rennes1.fr

[b] Dr. R. Gautier
UMR CNRS 6226—Sciences Chimiques de Rennes
Ecole Nationale Supérieure de Chimie de Rennes
Campus de Beaulieu, 35700 Rennes, (France)

## Results and Discussion

Figure 1 shows the X-ray powder diagrams of crushed single crystals of $Mo_{15}S_{19}$ before (bottom) and after a prolonged annealing at 700 °C (middle) in sealed silica tube. It is clear that the phase after annealing is totally different from the initial binary compound. As a consequence, we undertook an X-ray structural study on a single crystal. This study revealed that the new phase has the composition $Mo_{15}S_{20}$ and its crystal structure is based on the new unit $Mo_9S_{27}$ which coexists in equal proportion with the $Mo_6S_8$ unit as shown in Figure 2. The $Mo_9S_{27}$ moiety is shown in Figure 3. It can be viewed as resulting from the fusion of two $Mo_3S_{11}$ and three $MoS_6$ units. In fact it derives from the migration of the three

   

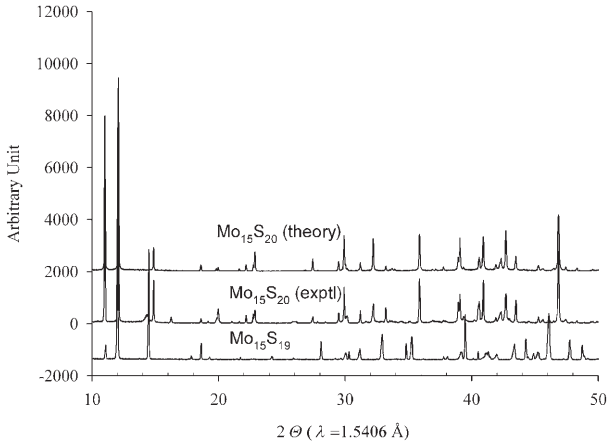


Figure 1. Experimental X-ray powder diffractograms of $Mo_{15}S_{19}$ (bottom) and $Mo_{15}S_{20}$ (middle). The theoretical diagram of $Mo_{15}S_{20}$ at the top was calculated from the refined crystal parameters.

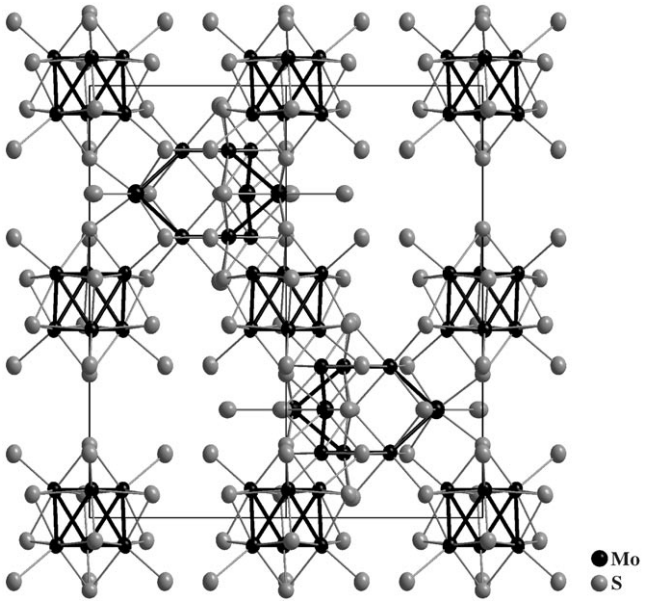


Figure 2. The crystal structure of $Mo_{15}S_{20}$. Thick lines denote Mo–Mo bonds and thin lines, Mo–S bonds.

Mo atoms of the median triangle of the bi-octahedral $Mo_9$ cluster found in $Mo_{15}S_{19}$ towards adjacent octahedral sites of sulfur atoms that are occupied by the trivalent indium ions in the precursor $In_{3.7}Mo_{15}S_{19}$ compound (cf. Figure 4). The Mo core of the $Mo_9S_{27}$ unit consists of two $Mo_3$ triangles (Mo2 atoms) forming an elongated prism, surrounding an interstitial sulfur atom (S6), with three additional Mo3 atoms bridging the edges of the rectangular faces. The Mo2–Mo2 distances along the edges of the triangles are 2.8512(4) Å, while those between the triangles are 3.5100(6) Å. The distances between the Mo2 atoms of the triangles and the bridging Mo3 atoms are 2.8766(4) Å. All the Mo atoms are surrounded by sulfur atoms forming distorted octahedra, with Mo–S distances in the range 2.3668(11)–2.7116(12) Å. The second unit, that is, the

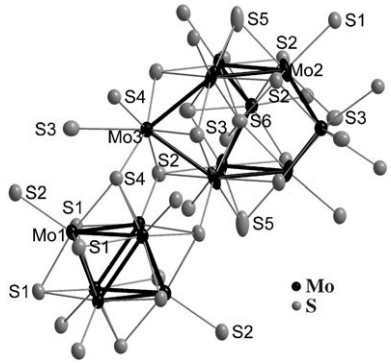


Figure 3. The $Mo_9S_{27}$ and $Mo_6S_8S_6$ units with the atomic labeling scheme. Selected distances (Å): Mo1–Mo1 2.7572(4), Mo1–Mo1 2.7700(4), Mo1–S1 2.4073(7), Mo1–S1 2.4172(7), Mo1–S4 2.4370(9), Mo1–S2 2.4570(7), Mo1–S1 2.4915(7), Mo2–Mo2 2.8512(4), Mo2–Mo3 2.8766(4), Mo2–S2 2.4051(7), Mo2–S6 2.4062(3), Mo2–S5 2.4441(11), Mo2–S3 2.4746(9), Mo2–S2 2.5902(7), Mo3–S3 2.3668(11), Mo3–S2 2.3901(7), Mo3–S4 2.4871(7), Mo3–S3 2.7116(12).

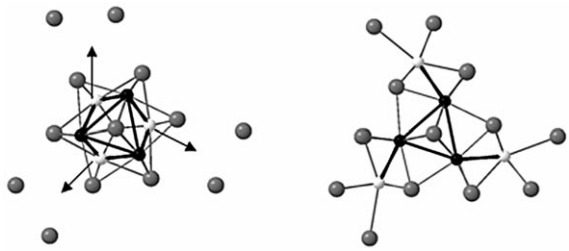

Figure 4. Process of formation of the $Mo_9S_{27}$ unit (right) by migration of the molybdenum atoms of the median triangle of the $Mo_9S_{17}$ unit (left).

$Mo_6S_8S_6$ unit, is similar to that encountered in the well-known Chevrel phases and can be described as a $Mo_6$ octahedron surrounded by eight face-capping inner $S^i$ (6 S1 and 2 S4) and six apical $S^a$ (S2) ligands. The Mo–Mo distances within the $Mo_6$ clusters are 2.7572 (4) for the intratriangle distances (distances within the Mo3 triangles formed by the Mo atoms related through the threefold axis) and 2.7700(4) Å for the intertriangle distances. The Mo–S bond lengths are in the range 2.4073(7)–2.4915(7) Å. Each $Mo_9S_{27}$ unit is interconnected to six $Mo_6S_8S_6$ units (and vice-versa) through Mo–S bonds (Figure 3) to form the three-dimensional Mo–S framework. From this arrangement, the shortest intercluster Mo1–Mo2 distance between the $Mo_6$ and $Mo_9$ clusters is 3.0652 (3) Å in the $Mo_{15}S_{20}$ compound.

Since Mo–Mo contacts between $Mo_6$ and $Mo_9$ units are rather long, as a first approximation, bonding in this compound can be tackled by considering the $Mo_6S_{14}$ and $Mo_9S_{27}$ clusters as isolated units. Previous studies have shown that the optimal ME count that corresponds to the occupation of bonding and nonbonding molecular orbitals (MOs) and vacancy of antibonding MOs, is equal to 24 for an octahedral $Mo_6S_{14}$ unit.[6] The electronic structure of $Mo_9S_{27}$ cluster of $C_{3h}$ symmetry can be formally analyzed as resulting from the interaction between the $(Mo_3)_2S_{18}$ prism and the three capping $MoS_3$ ligands. On the other hand, the MO diagram of

  

the $(Mo_3)_2S_{18}$ fragment itself can easily be derived from the one of the $Mo_3S_{11}$ triangular cluster. The MOs associated with M–M bonding in a $M_3L_{11}$ cluster are sketched on the left of Figure 5.[7] Since no metal–metal interaction occurs between the two $Mo_3$ units, the metallic part of the MO diagram of the $(Mo_3)_2S_{18}$ unit consists of six low-lying MOs and six higher MOs that derive from the three M–M bonding and three M–M antibonding orbitals of the $Mo_3$ triangle, respectively. The "$t_{2g}$" set of the $MoS_3$ fragments is sketched on the right of Figure 5. When brought together, the frontier MOs of the three $MoS_3$ groups give rise to a set of three combinations of the "$d_{z^2}$"-like MOs and six combinations coming from the doubly degenerate MOs of $MoS_3$. These last MOs interact mainly with the six Mo–Mo intra-$Mo_3$ antibonding orbitals, whereas the other three FMOs (fragment molecular orbitals) of the $(MoS_3)_3$ capping fragments interact with intra-$Mo_3$ Mo–Mo bonding MOs of the $(Mo_3)_2S_{18}$ fragment. These interactions results from overlap considerations between FMOs and are confirmed by extended Hückel (EH) calculations. Therefore, the resulting MO diagram of the isolated $Mo_9S_{27}$ presents twelve low-lying MOs with an overall Mo–Mo bonding character. These MOs are separated by a significant energetic gap (equal to about 0.5 eV according to EH calculations) from the three slightly antibonding MOs mainly centered on capping $MoS_3$ ligands. Therefore, the optimal count for such a unit is equal to 24 ME, which are distributed on the twelve Mo–Mo bonds. The experimental ME count is equal to 50. If a weak interaction occurs between the $Mo_6$ and $Mo_9$ clusters so that it can be considered as negligible in a first approximation, the two electrons, that remain when Mo–Mo bonding and nonbonding MOs of both clusters are occupied, must lie in Mo–Mo antibonding levels of one of the two clusters. Periodic density functional theory (DFT) calculations were carried out in order to study the intercluster interactions. Density of states (DOS) and crystal orbital Hamiltonian population (COHP) curves for different Mo–Mo contacts are sketched in Figure 6. The Fermi level cuts a DOS peak that is Mo–Mo nonbonding in the $Mo_6$ and $Mo_9$ clusters and has weak Mo–Mo intercluster antibonding. Integrated COHP of −0.127 and −0.103 Ry per unit cell are computed for Mo–Mo bonds of the $Mo_6$ and the $Mo_9$ clusters, respectively. An ICOHP value of −0.062 Ry per unit cell is computed for the Mo1–Mo2 intercluster bond. This shows that a significant interaction occurs between the clusters and that the above-mentioned approximation is probably too rough in this case, since Mo–Mo intercluster interaction is of the same order of magnitude as the Mo–Mo bonds of $Mo_6$ and $Mo_9$ units. Because of the weak intercluster Mo–Mo antibonding and intra-$Mo_6$ and intra-$Mo_9$ Mo–Mo nonbonding characters of the bands that just lie above the Fermi level, it should be possible to reduce the title compound without altering its architecture.

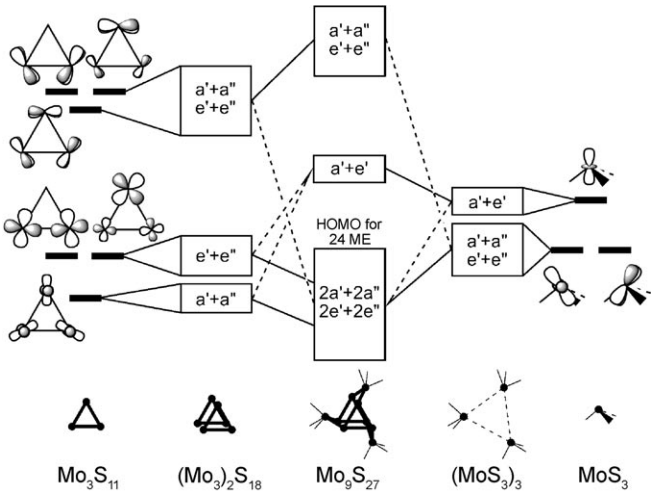


Figure 5. Qualitative MO diagrams based on EHT calculations for a) the $Mo_3S_{11}$ cluster, b) the $(Mo_3)_2S_{18}$ prismatic fragment, c) the $Mo_9S_{27}$ cluster, and d) the $(MoS_3)_3$ fragment. The FMOs of the $MoS_3$ fragment are shown on the far right side.

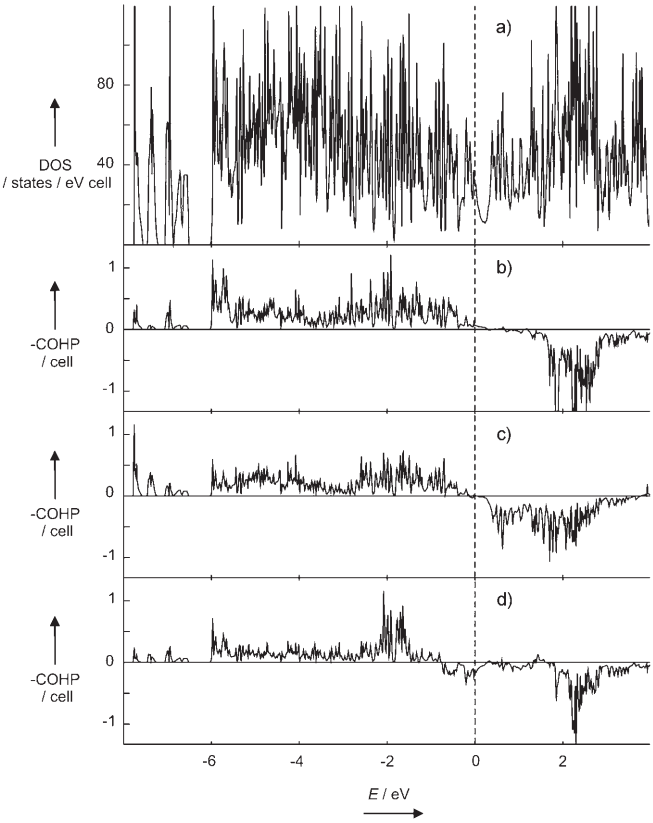


Figure 6. DFT calculations for $Mo_{15}S_{20}$: a) Total DOS and COHP for Mo-Mo bonds of ab) the $Mo_6$, c) the $Mo_9$ units, and d) for the Mo1–Mo2 intercluster bond.

According to the DFT DOS curve (Figure 6), metallic properties are envisioned for this compound. This was confirmed by susceptibility measurements on a batch of crystals (50 mg) which showed that $Mo_{15}S_{20}$ is a superconductor below 5 K (Figure 7).

  

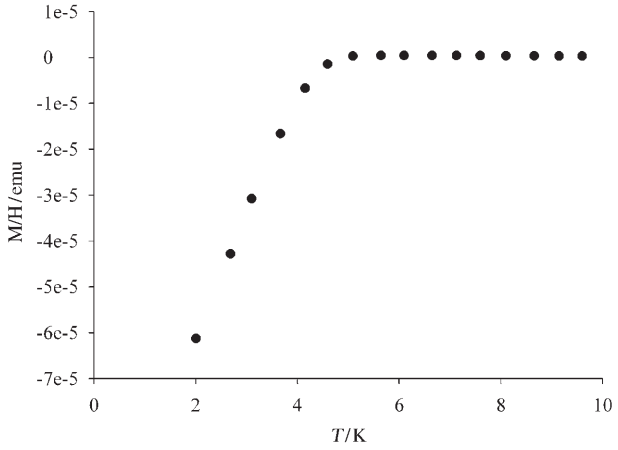


Figure 7. Temperature dependence of the magnetic susceptibility for $Mo_{15}S_{20}$. The magnetic field applied was 20 Oe.

## Experimental Section

**Preparation of $Mo_{15}S_{20}$**: The compound $Mo_{15}S_{20}$ was obtained in three steps. The first one was the synthesis of the solid-state compound $In_{3.7}Mo_{15}S_{19}$, followed by obtaining the binary $Mo_{15}S_{19}$ by "chimie douce" and, finally the synthesis of the title compounds by prolonged annealing at 700 °C. All these steps were performed on single crystals.

$In_{3.7}Mo_{15}S_{19}$ was synthesized from a stoichiometric mixture of $MoS_2$, $In_2S_3$ and Mo, all in powder form. To avoid any contamination by oxygen and moisture, the starting reagents were mixed, ground together in a mortar and then cold-pressed in a purified argon-filled glove box. The pellet (ca. 3 g) of the starting reagents was then loaded in a silica ampoule, which was then sealed under a dynamic vacuum of about $10^{-2}$ Pa. The ampoule was heated at a rate of 50 °C $h^{-1}$ up to 1120 °C and held there for 48 h, then cooled at 100 °C $h^{-1}$ to 1000 °C and finally cooled down to room temperature in the furnace. The resulting product was found as a pure phase on the basis of its X-ray powder diffraction diagram. Single crystals suitable for X-ray structural studies were obtained at 1050 °C by using In metal in excess.

Single crystals of the binary compound $Mo_{15}S_{19}$ were obtained from oxidation of single-crystals of $In_{3.7}Mo_{15}S_{19}$ by iodine in silica tube sealed under vacuum. The end of the tube containing the crystals of the indium compounds and an excess of iodine was placed in a furnace with about 3 cm of the other end sticking out of the furnace, at about room temperature. The furnace was then heated at 300 °C for 96 h. At the end of the reaction, crystals of $InI_3$ and $I_2$ were obtained at the cool end of the tube.

Single crystals of $Mo_{15}S_{20}$ were obtained by prolonged annealing, up to 45 days, of single crystals of $Mo_{15}S_{19}$ at 700 °C in silica ampoule sealed under vacuum. The new binary phase is stable up to 750 °C, temperature at which it decomposes into $Mo_2S_3$ and Mo.

**Magnetic measurements**: Magnetic susceptibility data of $Mo_{15}S_{20}$ were collected on a SHE-906 SQUID magnetosusceptometer under a magnetic field of 20 G.

**Crystal structure data for $Mo_{15}S_{20}$**: Hexagonal, space group $P6_3/m$ (no. 176), $a = 9.2473(2)$, $c = 17.5943(2)$ Å, $V = 1302.96(4)$ Å$^3$, $Z = 2$, $\rho_{calcd} = 5.302$ Mg m$^{-3}$, $F(000) = 1900$, $\lambda(Mo_{K\alpha}) = 0.71073$ Å, $\mu(Mo_{K\alpha}) = 8.541$ mm$^{-1}$, $T = 20$ °C. A black hexagonal crystal of approximate dimensions $0.09 \times 0.08 \times 0.07$ mm$^3$ was employed in the intensity data collection conducted with a Nonius KappaCCD diffractometer. The COLLECT program package[8] was used to establish the angular scan conditions ($\phi$ and $\omega$ scans) used in the data collection. A total of 508 frames were collected with a frame width of 0.8° and an exposure time of 30 s. Reflection indexing, Lorentz-polarization correction, peak integration, and background determination were performed by using the EvalCCD program.[9] An absorption correction (min/max transmission = 0.5744/0.6063) was applied using the description of the crystal faces.[10] Of 24190 reflections collected in the 3.44–39.76° $\theta$ range, 2715 were independent ($R_{int} = 0.0516$). The structure was solved with SIR97,[11] and revealed the three Mo and the six S atoms forming the crystal structure of $Mo_{15}S_{20}$. Refinement of this model using SHELXL[12] lead to a value $R = 0.0655$. At this stage, a difference Fourier synthesis revealed two peaks of 23 and 18 e Å$^{-3}$ which correspond to the position of the Mo3 and Mo2 atoms forming the $Mo_9$ cluster in the parent structure $Mo_{15}S_{19}$, which also crystallizes in the space group $P6_3/m$. This clearly indicates the existence of a small amount of the starting phase in the crystal investigated despite the fact that it was annealed during 45 days at 700 °C. Consequently, subsequent refinements were made on a model that simultaneously including both $Mo_{15}S_{20}$ and $Mo_{15}S_{19}$ phases. To take into account the percentage of the two phases in the crystal, two overall occupancy factors, the sum of which was constrained to the unity, were ascribed to all atoms of the phases $Mo_{15}S_{20}$ and $Mo_{15}S_{19}$. The positional and atomic displacement parameters of the Mo and S atoms forming the $Mo_6S_8$ unit that is common to both structures were refined dependently. Refinement of this model led to the final values $R_1 = 0.0306$, $wR_2 = 0.0684$ for the 2407 reflections with $I > 2\sigma(I)$. The ratio between the phases $Mo_{15}S_{20}$ and $Mo_{15}S_{19}$ was 92.5(1):7.5(1). The final electron density difference map was flat with a maximum of 1.66 e Å$^3$ and a minimum of $-1.87$ e Å$^3$. Refinements with the multiphase option in Jana2000,[13] which used combination of two phases as if they diffract independently, failed because the second domain was completely cancelled. This proves that the disorder effect takes place within a coherent region. In addition, as the $c$ parameter of the starting binary $Mo_{15}S_{19}$ is 1.08 times greater than that of $Mo_{15}S_{20}$, we made a reconstruction of the ($0kl$) reciprocal plane to see the possible existence of split or overlapping reflections and if all reflections were indexed with the parameters $a = 9.2473(2)$ and $c = 17.5943(2)$ Å. The Figure 8 shows that all reflections are indexed with these parameters (cir-

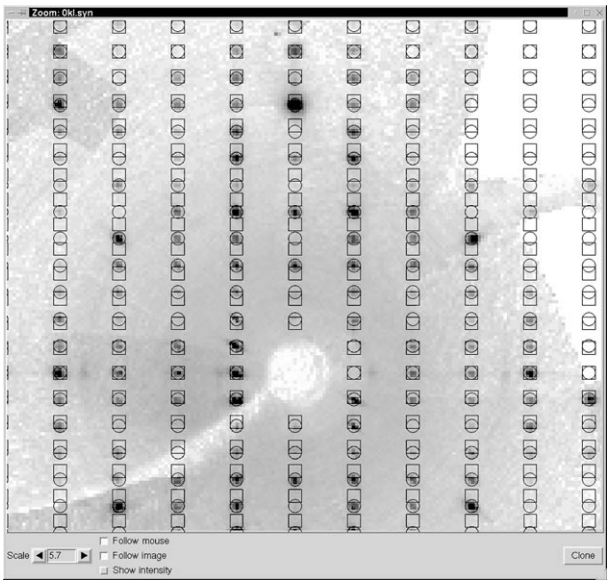


Figure 8. Reconstructed precession image of the ($0kl$) reciprocal plane.

cles in Figure 8) and no reflections were observed at the position corresponding to the $c$ parameter of the starting $Mo_{15}S_{19}$ (squares). This shows clearly that the two components of the crystal have the same unit-cell parameters. In particular, it is interesting to note that during the decomposition process, the $c$ parameter of the unit cell of $Mo_{15}S_{19}$ contracts by 7.7% and the $a$ parameter expands by 0.7%. Further details of the crystal structure investigation may be obtained from the Fachinformationszentrum Karlsruhe, D-76344 Eggenstein-Leopoldshafen, Germany (fax: (+49)7247–808–666; e-mail: crysdata@fiz-karlsruhe.de), on quoting the depository number CSD-416352.

  

**Computational methods**: Extended Hückel[14] calculations were carried out by using the program CACAO.[15] The exponents ($\xi$) and the valence shell ionization potentials (Hii in eV) were (respectively): 2.275, −32.3 for S 3s; 1.817, −13.3 for S 3p; 1.956, −8.34 for Mo 5s; 1.921, −5.24 for Mo 5p. Hii values for Mo 4d were set equal to −10.50. A linear combination of two Slater-type orbitals of exponents $\zeta_1 = 4.542$ and $\zeta_2 = 1.901$ with the weighting coefficients $c_1 = c_2 = 0.5898$ was used to represent the Mo 4d atomic orbitals. Self-consistent ab initio band structure calculations were performed with the scalar relativistic tight-binding linear muffin-tin orbital (LMTO) method in the atomic spheres approximation including the combined correction.[16] Exchange and correlation were treated in the local density approximation using the von Barth–Hedin local exchange correlation potential.[17] Within the LMTO formalism interatomic spaces are filled with interstitial spheres. The optimal positions and radii of these additional "empty spheres" (ES) were determined by the procedure described in reference [18]. Ten non-symmetry-related ES with $0.83 \leq r_{ES} \leq 2.30$ Å were introduced for the calculations. The full LMTO basis set consisted of 5s, 5p, 4d and 4f functions for Mo spheres, 3, 3p, and 3d for S spheres, and s, p, and d functions for ES. The eigenvalue problem was solved using the following minimal basis set obtained from the Löwdin downfolding technique: Mo 5s, 5p, 4d; S 3 s, 3p; and interstitial 1s LMTOs. The $k$ space integration was performed using the tetrahedron method.[19] Charge self-consistency and the average properties were obtained from 117 irreducible $k$ points. A measure of the magnitude of the bonding was obtained by computing the crystal orbital Hamiltonian populations (COHP), which are the Hamiltonian population weighted density of states (DOS).[20,21] As recommended, a reduced basis set (in which all ES LMTOs have been downfolded) was used for the COHP calculations.[22] DOS and COHP curves were shifted so that $\varepsilon_F$ lies at 0 eV.

[1] a) Superconductivity in Ternary Compounds, Vol. I, II (Eds.: M. B. Maple, Ø. Fischer), Springer, Berlin, **1982** (*Top. Curr. Phys.* **1982**, 32); R. Chevrel, P. Gougeon, M. Potel, M. Sergent, *J. Solid State Chem.* **1985**, *57*, 25.

[2] a) J. C. Armici, M. Decroux, O. Fischer, M. Potel, R. Chevrel, M. Sergent, *Solid State Commun.* **1980**, *33*, 607–611; b) R. Lepetit, P. Monceau, M. Potel, P. Gougeon, M. Sergent, *J. Low Temp. Phys.* **1984**, *56*, 219–235; c) R. Brusetti, O. Laborde, A. Sulpice, R. Calemczuk, M. Potel, P. Gougeon, *Phys. Rev. B* **1995**, *52*, 4481–4493.

[3] P. Gougeon, M. Potel, J. Padiou, M. Sergent , C. Boulanger, J.-M. Lecuire, *J. Solid State Chem.* **1987**, *71*, 543.

[4] M. Potel, P. Gougeon, R. Chevrel , M. Sergent, *Rev. Chim. Min.* **1984**, *21*, 509.

[5] D. Salloum, R. Gautier, P. Gougeon, M. Potel, *J. Solid State Chem.* **2004**, *177*, 1672.

[6] a) T. Hughbanks, R. Hoffmann, *J. Am. Chem. Soc.* **1983**, *105*, 1150; b) T. Hughbanks, *Prog. Solid State Chem.* **1989**, *19*, 329.

[7] Y. Jiang, A. Tang, R. Hoffmann, J. Huang, J. Lu, *Organometallics* **1985**, *4*, 27.

[8] Nonius BV, COLLECT, data collection software, Nonius BV, **1999**.

[9] A. J. M. Duisenberg, Ph.D. thesis, University of Utrecht (NL), **1998**.

[10] J. de Meulenaar, H. Tompa, *Acta Crystallogr. Sect. A* **1965**, *19*, 1014.

[11] A. Altomare, M. C. Burla, M. Camalli, G. L. Cascarano, C. Giacovazzo, A. Guagliardi, A. G. G. Moliterni, G. Polidori, R. Spagna, *J. Appl. Crystallogr.* **1999**, *32*, 115.

[12] G. M. Sheldrick, SHELXL97, Universität Göttingen, Göttingen (Germany) **1997**.

[13] V. Petricek, M. Dusek, L. Palatinus, Jana 2000. The crystallographic computing system, Institute of Physics, Praha (Czech Republic), **2000**.

[14] R. Hoffmann *J. Chem. Phys.* **1963**, *39*, 1397.

[15] C. Mealli, D. Proserpio, *J. Chem. Educ.* **1990**, *67*, 399.

[16] a) O. K. Andersen, *Phys. Rev. B* **1975**, *12*, 3060; b) O. K. Andersen, *Europhys. News* **1981**, *12*, 4; c) O. K. Andersen, in *The Electronic Structure Of Complex Systems* (Eds.: P. Phariseau, W. M. Temmerman), Plenum, New York, **1984**; d) O. K. Andersen, O. Jepsen, *Phys. Rev. Lett.* **1984**, *53*, 2571; e) O. K. Andersen, O. Jepsen, M. Sob, in , *Electronic Band Structure and Its Application* (Ed.: M. Yussouf), Springer, Berlin, **1986**; f) H. L. Skriver, *The LMTO Method*, Springer, Berlin, **1984**.

[17] U. von Barth, L. Hedin, *J. Phys.* **1972**, *5*, 1629.

[18] O. Jepsen, O. K. Andersen, *Z. Phys. B* **1995**, *97*, 35.

[19] P. E. Blöchl, O. Jepsen, O. K. Andersen, *Phys. Rev. B* **1994**, *49*, 16223.

[20] R. Dronskowski, P. E. Blöchl, *J. Phys. Chem.* **1993**, *97*, 8617.

[21] F. Boucher, R. Rousseau, *Inorg. Chem.* **1998**, *37*, 2351.

[22] O. Jepsen, O. K. Andersen, personal communication.

Received: September 1, 2006
Published online: September 29, 2006

  